CO Adsorption on Pd Nanoparticles: Density Functional and Vibrational Spectroscopy Studies

Ilya V. Yudanov,† Riadh Sahnoun, Konstantin M. Neyman,* and Notker Rösch

Institut für Physikalische und Theoretische Chemie, Technische Universität München, 85747 Garching, Germany

Jens Hoffmann, Swetlana Schauermann, Viktor Johánek, Holger Unterhalt, Günther Rupprechter, Jörg Libuda, and Hans-Joachim Freund

Fritz-Haber-Institut der Max-Planck-Gesellschaft, Faradayweg 4-6, 14195 Berlin, Germany

Received: September 11, 2002; In Final Form: October 29, 2002

Adsorption of CO on nanosize Pd particles was studied theoretically by density functional method and spectroscopically by means of infrared reflection absorption spectroscopy (IRAS) and sum frequency generation (SFG). A density functional approach was applied to three-dimensional crystallites of about 140 atoms. The model clusters were chosen as octahedral fragments of the face centered cubic (fcc) bulk, exhibiting (111) and (001) facets. Bare and adsorbate-decorated cluster models were calculated with O_h symmetry constraints. Various types of adsorption sites were inspected: 3-fold hollow, bridge, and on-top positions at (111) facets; 4-fold hollow and on-top sites at (001) facets; bridge positions at cluster edges; on-top positions at cluster corners; and on single Pd atoms deposited at regular (111) facets. Adsorption properties of the relatively small regular cluster facets (111) and (001) are calculated similar to those of corresponding ideal (infinite) Pd surfaces. However, the strongest CO bonding was calculated for the bridge positions at cluster edges. The energy of adsorption on-top of low-coordinated Pd centers (kinks) is also larger than that for on-top sites of (111) and (001) facets. To correlate the theoretical results with spectroscopic data, vibrational spectra of CO adsorbed on supported Pd nanocrystallites of different size and structure (well-faceted and defect-rich) were measured using IRAS and SFG. For CO adsorption under ultrahigh vacuum conditions, a characteristic absorption in the frequency region 1950−1970 cm^{-1} was observed, which in agreement with the theoretical data was assigned to vibrations of bridge-bonded CO at particle edges and defects. SFG studies carried out at CO pressures up to 200 mbar showed that the edge-related species was still present under catalytic reaction conditions. By decomposition of methanol leading to the formation of carbon species, these sites can be selectively modified. As a result, CO occupies on-top positions at particle edges and defects. On the basis of the computational data, the experimentally observed differences in CO adsorption on alumina-supported Pd nanoparticles of different size and surface quality are interpreted. Differences between adsorption properties of Pd nanoparticles with a large fraction of (111) facets and adsorption properties of an ideal Pd(111) surface are also discussed.

1. Introduction

Clusters constitute an intermediate state of matter between isolated molecular species and solids.[1,2] Physical and chemical properties of clusters are size-dependent[3] and thus tunable. This is particularly important for the synthesis of nanostructured materials[2] and for heterogeneous catalysis by transition metals.[4,5] Modern experimental techniques permit us to design and characterize model catalysts in the form of metal nanoparticles of well-defined structure, grown on oxide surfaces. For instance, recently, palladium nanoclusters supported on thin alumina and silica films and their characteristics for adsorption and oxidation of CO were intensively studied.[6−12] It was observed that in many cases clusters grown on an alumina film exhibit a well-faceted truncated fcc structure with a large fraction of (111) facets.[6−11] At low CO pressure, the adsorption site occupancy was found to depend on particle size, surface structure, and temperature.[6,10,11] On well-faceted Pd particles, CO preferentially adsorbs at bridge sites, whereas on more defective Pd particles, i.e., on smaller or less-ordered particles, a significant fraction of on-top sites is observed as well. Even well-faceted Pd particles exhibit adsorption properties similar to those of defect-rich Pd(111) surface rather than of an ideal Pd(111) surface.[10,11]

Carbon monoxide is, on one hand, a touchstone adsorbate; on the other hand, it is a key reagent in methanol synthesis over oxide-supported Pd catalysts.[13] On the basis of vibrational spectroscopy data, CO is known to adsorb at 3-fold hollow sites of well-prepared Pd(111) surfaces when the coverage is up to half a monolayer, $\theta \leq 0.5$.[10,11] Around $\theta = 0.6-0.7$, CO is preferentially bridge-bonded (C−O stretching frequency ∼1960 cm^{-1}) with a small amount of on-top sites occupied (∼2090 cm^{-1}).[10,11] Further coverage increase leads to decreasing intensity of the bridge-bonded peak, and at coverage $\theta = 0.75$ an ordered structure (2×2) forms, manifested by two intense

* Corresponding author. Fax: +49+89-289-13622. E-mail: neyman@ch.tum.de.

† Permanent address: Boreskov Institute of Catalysis, 630090 Novosibirsk, Russia.

10.1021/jp022052b CCC: $25.00
Published on Web 12/10/2002

vibrational bands at 1895 and 2110 cm^{-1}.[14] Density functional (DF) slab model calculations show that for this (2×2)-3 CO structure fcc, hcp 3-fold sites as well as on-top sites (each per 2×2 unit cell) are energetically preferred to occupation of one on-top and two 2-fold bridge sites.[15] Thus, on the ideal Pd(111) surface, bridge sites are occupied only in the relatively narrow CO coverage range from $\theta = 0.6$ to $\theta = 0.7$. Coverage $\theta = 0.6$ is reached at a CO pressure of 10^{-6} mbar at 190 K and at 100 mbar at 300 K. On the other hand, for alumina-supported Pd nanoparticles a strong signal of bridge-bonded CO is present already for a pressure of 10^{-7} mbar at 300 K.[10] Also, on nanoparticles the vibrational peak around 1975 cm^{-1} is characteristic for CO bridge-bonded at defect-rich (stepped) Pd(111) facets whereas it is observed at 1955 cm^{-1} for CO bridge-bonded at perfect (111) terraces.[10,11] Small Pd particles with a mean size of 3.5 nm grown at 90 K exhibit a rough surface with many defects and no distinct facets.[10,11] The vibrational peak observed for CO on these small clusters around 1975 cm^{-1} also clearly indicates the defect-related nature of the bridge sites on these particles.[10,11] Another feature differentiating supported Pd nanoparticles from the ideal Pd(111) surface is occupation of on-top positions ($\sim$2100 cm^{-1}) at low pressures: on the Pd(111) surface the corresponding CO peak appears only at $\theta > 0.6$.

Previously, some of us investigated octahedral and cuboctahedral palladium nanoclusters, ranging from Pd_{55} to Pd_{146}, by means of all-electron relativistic DF calculations.[16] In particular, we focused on the interaction of CO with 3-fold hollow sites located at the center of (111) facets (a single CO molecule per facet) and we analyzed how calculated adsorption parameters vary with cluster size. We also examined how observables calculated for that adsorption position on cluster facets relate to adsorption properties of the corresponding site at a single-crystal surface Pd(111). We were able to demonstrate that cluster models of about 80 and more Pd atoms describe various adsorption properties of the Pd(111) surface (including the adsorption energy) with quantitative accuracy.[16] In the present study, we theoretically address CO adsorption at other sites of Pd nanoparticles, such as edges, corners, or defect atoms deposited on the regular cluster facets. In most cases, the adsorbed CO molecules have been considered at cluster positions that are far enough from each other so that a direct adsorbate−adsorbate interaction is negligible; thus, our results correspond to experimental ultrahigh vacuum conditions at sufficiently low CO coverage. With the calculated adsorption parameters of Pd nanoclusters we intend to shed light on two important issues: (i) how adsorption characteristics of metal particles (that also exhibit several adsorption sites) change with cluster size, and (ii) how adsorption properties of supported Pd nanoparticles differ from those of the well-ordered Pd(111) surface.

A correlation of the theoretical data on the adsorption of CO on Pd nanoparticles with experimental results requires the preparation of nanoparticle systems, which can be experimentally investigated in great detail. As mentioned above, this is the case for so-called supported *model catalysts*, which in contrast to real catalysts reveal a reduced complexity and can be easily studied using most surface science techniques.[5,17−19] In this work, we employed Pd model catalysts supported by an ordered Al_2O_3 film grown on NiAl(110).[20,21] Previously, this system has been characterized in detail with respect to its electronic and geometric structure as well as its adsorption properties (see ref 4 and references therein). In addition, the kinetics and mechanism of several model reactions have been investigated.[10,11,22−24] To probe different adsorption sites, we performed vibrational spectroscopy measurements of CO adsorbed on the Pd nanoparticles employing two types of experimental techniques. Under UHV (ultrahigh vacuum) conditions, infrared reflection absorption spectroscopy (IRAS) was applied.[22] Using sum frequency generation (SFG),[6,10,11] vibrational spectra can be acquired from UHV up to ambient conditions, allowing us to examine whether UHV results can be transferred to a technically relevant higher pressure range.

2. Computational

The calculations were carried out at the all-electron level using the linear combination of Gaussian-type orbitals fitting-functions density functional (LCGTO-FF-DF) method[25] as implemented in the parallel code ParaGauss.[26,27] We used the scalar relativistic variant of the LCGTO-FF-DF method which employs a second-order Douglas-Kroll transformation to decouple electronic and positronic degrees of freedom of the Dirac−Kohn−Sham equation.[28,29]

Self-consistent solutions of the Kohn−Sham equations were obtained within the local density approximation (LDA; VWN parametrization[30]). To study CO adsorption, we evaluated energies in a generalized-gradient approximation (GGA, BP86 exchange-correlation functional[31,32]) using the electron density of self-consistent LDA calculations; this computational strategy is very economic, yet sufficiently accurate.[33] In some cases explicitly specified in the following, we also employed the PBEN[34] GGA functional for comparison with BP86 results.

For Pd, we used a Gaussian-type orbital basis set[35] extended to (18*s*,13*p*,9*d*) by adding one *s* exponent (0.0135), two *p* exponents (0.0904 and 0.0214), and one *d* exponent (0.097). This basis set was contracted to [7*s*,6*p*,4*d*] using relativistic VWN atomic eigenvectors. To evaluate the classical Coulomb contribution to the electron−electron interaction, the electron density was represented with the help of an auxiliary basis set.[25] The exponents of *s* and r^2 type fitting functions were generated from the orbital basis set by a standard procedure;[25] in addition, we chose the *p* and *d* "polarization exponents" as geometric series with factor 2.5, starting with 0.1 and 0.2 for *p* and *d* exponents, respectively. For Pd, the auxiliary basis set was of the size (17*s*,6r^2,5*p*,5*d*). C and O atoms were described by orbital basis sets of quality (14*s*,9*p*,4*d*)[36] using the original general contraction [6*s*,5*p*,2*d*] and by auxiliary charge density basis sets (14*s*,9r^2,5*p*,5*d*).

Since spin-polarized test calculations for selected Pd clusters revealed no unpaired electrons, we will discuss only results of spin-restricted calculations in the following. To ensure convergence of the electron density during the SCF procedure, we applied throughout a technique of fractional occupation numbers with a level broadening of 0.1 eV.[25] For all Pd clusters, we used an experimental bulk-terminated geometry with a Pd−Pd distance of 2.75 Å.[37] In some cases (Section 4.1.2), we carried out full geometry optimization (subject only to O_h symmetry restrictions) of bare Pd clusters at the LDA level, invoking a quasi-Newton algorithm and analytical forces.[38,39] Finally, the GGA energy functional was evaluated for LDA-optimized clusters (BP86//VWN).

In the calculations of CO adsorption, we kept all Pd atoms at positions corresponding to bare cluster, i.e., we neglected adsorbate-induced relaxation. To obtain approximate equilibrium geometries of adsorption complexes with CO molecules oriented according to the symmetry group O_h, we consecutively varied Pd−C and C−O distances until deviations were below 0.001 Å, using BP86 energies. We corrected the CO adsorption energy for the basis set superposition error via the standard counterpoise

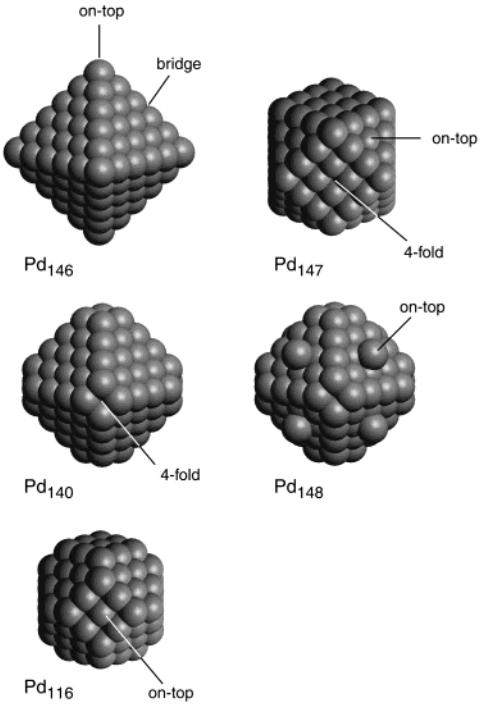

Figure 1. Model Pd nanoparticles of O_h symmetry.

technique.[40] To estimate the harmonic CO vibrational frequency, we approximated the C−O internal mode by keeping the CO center of mass fixed; polynomials of degree 4 and 3 were fitted to five total energy values near the minimum of the potential curve. Both polynomials give essentially the same value of harmonic frequency; we neglected the anharmonic correction from the third-order polynomial fitting, which is almost constant (23−26 cm^{-1}) and close to the experimental value for a free CO molecule.

We selected a series of metal clusters of O_h symmetry—Pd_{116}, Pd_{140}, Pd_{146}, Pd_{147}, Pd_{148} (Figure 1). These are particles with dimensions ranging from ∼1.4 nm (Pd_{116}) to ∼1.9 nm (Pd_{146}). Due to their high symmetry, the electronic structure of these clusters is determined by a rather moderate number of symmetry-nonequivalent Pd centers. For instance, each of the largest clusters Pd_{146} and Pd_{147} comprises only nine nonequivalent Pd atoms. This is to some extent reminiscent of calculations with periodic boundary conditions where a relatively small elementary cell is used to describe an infinite crystal structure. Highly symmetric (three-dimensional) cluster models contain a considerably larger fraction of Pd atoms with high coordination numbers compared to "planar" ("two-dimensional") cluster models, commonly used in chemisorption studies.[41,42] Boundary metal atoms of such conventional cluster models are a source of inaccuracy in calculations of chemisorption complexes. On the other hand, boundary atoms of three-dimensional cluster models utilized here (Figure 1) are described considerably more realistically.[16] The program ParaGauss[26,27] allows full exploitation of the high symmetry and thus makes such large heavy-metal particles computationally tractable, even at the accurate all-electron scalar relativistic level adopted here.

Cluster Pd_{146} in Figure 1 is of ideal octahedral shape with eight hexagonal (111) facets. This cluster is constructed by successive deposition of octahedral shells of Pd atoms around a central Pd_6 unit: completion of the first shell produces the cluster Pd_{44}, an additional shell leads to Pd_{146}. The cuboctahedral clusters Pd_{116} and Pd_{140} (Figure 1) are obtained by truncating the octahedral cluster Pd_{146} along the planes (100), (010), and (001). First, six corner atoms are removed resulting in Pd_{140}; this cluster exhibits also six smallest (001) facets comprised of 4 atoms. Next, the top layer of each tetragonal facet of Pd_{140} is removed to yield the cluster Pd_{116}. Similarly, Pd_{147} is obtained by truncating the full octahedron Pd_{231}. Cluster Pd_{148} was used to study kink defects at (111) facets, which are represented by Pd atoms deposited at 3-fold hollow sites in the center of each (111) facet of Pd_{140}.

3. Experimental Section

The IRAS experiments were performed in a combined molecular beam/IRAS apparatus developed at the Fritz-Haber-Institute (Berlin).[43] Briefly, the system combines several independent beam sources, angular-resolved and -integrated gas-phase detection, and in-situ time-resolved IRAS. SFG experiments were performed in a UHV surface analysis system combined with an SFG-compatible UHV-high-pressure cell, as described in refs 9 and 44. For details about SFG spectroscopy we refer to the literature[9,45] (and references therein).

The alumina film was prepared by sputtering and annealing of a NiAl(110) single crystal, followed by an oxidation and annealing procedure.[21,46] Cleanliness and quality of the oxide film was checked via LEED (low-energy electron diffraction) and AES (Auger electron spectroscopy). Before the experiment, Pd (>99.9%) was deposited using a commercial evaporator (Focus, EFM 3). Details concerning the preparation conditions were given elsewhere.[10,47] After preparation, the Pd particles were stabilized by oxygen and CO exposure as discussed previously.[48,49] The IR spectra displayed were acquired using a vacuum FT-IR spectrometer (Bruker) at a spectral resolution of 2 cm^{-1} and at a sample temperature of 100 K. For the IR spectra shown in the following, the samples were saturated with CO at 300 K by exposure to a dose of approximately 20 L (1 L = 10^{-6} Torr s), generated from an effusive beam source. Partially carbon-covered surfaces were prepared by extended exposure to methanol (approximately 7000 L) via an effusive beam source at a sample temperature of 440 K.[23,24]

4. Results and Discussion

4.1. Calculated Energetics of CO Adsorption on Pd Nanoclusters. *4.1.1. CO Adsorption at (111) Facets.* Well-ordered Pd nanoparticles grown on alumina film deposited on NiAl alloy exhibit mainly (111) and (100) surface facets.[10,11] The (111) top facet (parallel to the oxide substrate surface) dominates the particle morphology and the fraction of side (111) and (100) facets is assumed to be small.[10] Therefore, let us start by considering CO adsorption at regular (111) facets of Pd clusters. From experimental investigations as well as from periodic slab model calculations it is known that the 3-fold hollow site on the Pd(111) surface is favored for CO adsorption at low coverage.[15,50−52] Previously, some of us theoretically investigated CO adsorption at hollow sites located at the center of (111) facet for two series of octahedral clusters:[16] Pd_{55}, Pd_{79}, Pd_{85}, and Pd_{116}, Pd_{140}, Pd_{146}. The adsorbed CO molecules (one per facet) were placed in a symmetric fashion at central sites of each of the eight (111) facets. This is the fcc hollow site for the first cluster series (with a subsurface octahedral hole beneath the site) and the hcp site for the second series (tetrahedral subsurface hole).

The calculations[16] yielded rather uniform interatomic distances, vibrational frequencies, and adsorption energies for all cluster models—with the exception of the smallest one, Pd_{55}, that features incomplete coordination of the three palladium atoms forming the hollow site. In particular, for clusters larger than Pd_{55}, the adsorption energy per CO molecule (at the BP86

TABLE 1: Calculated Properties of CO Adsorbed on Different Sites of Regular (111) Facets of the Clusters Pd_{146} (hcp, bridge, and on-top) and Pd_{147} (on-top)

	hcp		bridge	on-top	
	$Pd_{146}(CO)_8$	$Pd_{146}(CO)_{24}$	$Pd_{146}(CO)_{24}$	$Pd_{146}(CO)_{24}$	$Pd_{147}(CO)_8$
r(C−O), Å	1.188	1.183	1.171	1.152	1.152
r(Pd−C), Å	2.067	2.100	2.046	1.854	1.884
D_e(BP86),[a] eV	1.77	1.69	1.47	1.15	1.16
D_e(PBEN//BP86),[b] eV	1.49	1.38	1.18	0.92	0.93
ν_e(C−O),[c] cm^{-1}	1755	1803	1876	2012	1987
ν_e(C−O) × 1.04,[d] cm^{-1}	1825	1875	1951	2092	2066

[a] Adsorption energy from a relativistic BP86 calculation. [b] Relativistic PBEN adsorption energy calculated with BP86 geometry. [c] Calculated harmonic frequency of C−O vibration. [d] Scaled vibrational CO frequency, see text.

level) varies in a very narrow interval, from 1.77 to 1.82 eV; the computed CO adsorption parameters for the largest cluster of the series, $Pd_{146}(CO)_8$, are given in Table 1. Thus, significant cluster size effects are already eliminated for symmetric three-dimensional models that contain about 80 Pd atoms. Results of this investigation demonstrated[16] that convergence of adsorption energies on metals can be reached for moderately large cluster models, provided that these models feature a compact shape terminated by low-index crystal facets. We assume the difference in adsorption energies between fcc and hcp positions to be smaller than cluster size effects and thus we will neglect it in the following discussion. Indeed, slab model calculations for the ideal Pd(111) surface show that the difference in CO adsorption energy at the two 3-fold hollow sites, fcc and hcp, is very small (0.03 eV[15] or less than 0.01 eV[52]).

At variance with the aforementioned clusters with hollow-centered (111) facets, the cluster Pd_{147} (Figure 1) exhibits on-top positions at the center of (111) facets. Calculated adsorption parameters for $Pd_{147}(CO)_8$ are given in Table 1. Not unexpectedly, the binding energy for on-top CO is notably weaker than that for 3-fold hollow sites. Concomitantly, a longer Pd−C distance and smaller C−O frequency shift (with respect to gas-phase CO) are calculated for this on-top adsorption complex.

It is instructive to compare the results for hollow and on-top positions located in the centers of (111) facets, i.e., most remote from cluster edges and corners, with results obtained for slab models of the ideal Pd(111) surface. Recently, adsorption of CO on Pd(111) surface was studied in detail employing slab models and the PW91 exchange-correlation functional.[15] At low coverage ($\theta = 1/3$), the adsorption energies for hcp hollow and on-top sites were calculated at 1.98 and 1.36 eV, respectively.[15] The fcc site, with a binding energy of 2.01 eV, is only slightly more stable than the hcp site.[15] The adsorption energy at a bridge site was calculated at 1.81 eV, weaker than the interaction at both hollow sites.[15] Thus, the energy difference, 0.61 eV, between hcp and on-top positions in our cluster calculations at the BP86 level (Table 1) agrees with the PW91 slab model result. To compare absolute values of adsorption energies, we also carried out PW91 calculation of CO adsorption complex on the hcp-hollow sites of cluster Pd_{146}. Optimized geometry parameters, r(Pd−C) = 2.063 Å and r(C−O) = 1.187 Å, hardly changed with respect to the BP86 data (Table 1). As anticipated,[53] the PW91 adsorption energy, 1.95 eV, is higher than the BP86 energy. Taking into account the differences in computational parameters used in the cluster and slab model studies (in particular, the geometry of the Pd substrate[16]), one can conclude that the adsorption energies of the present model cluster calculations are in *quantitative agreement* with results of the periodic slab model calculations. This holds despite the fundamental methodological differences between the cluster code ParaGauss and the slab model codes; we mention in particular the all-electron scalar relativistic description based on localized basis functions in our work[28] and the ultra-soft pseudopotentials combined with a plane-wave representation of orbitals in the slab model calculations.[15,52] Good agreement between the cluster and slab model results implies that the properties of adsorption sites located close to the middle of regular (111) facets for the clusters of about 100 Pd atoms (considered at fixed bulk terminated geometry) do not much differ from the properties of ideal Pd(111) surface. We expect our cluster models to achieve comparable accuracy with regard to experimental values for larger well-ordered Pd particles.

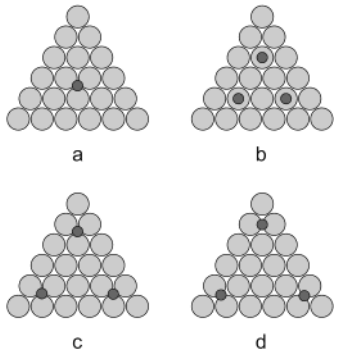

Figure 2. Different modes of CO adsorbate deposition at (111) facets of the cluster Pd_{146}: (a) central hcp position; (b) three on-top positions; (c) three hcp hollow sites; (d) three bridge positions.

Another important aspect is how the adsorption energy calculated with different exchange-correlation functionals corresponds to the experimental measurements. The BP86 adsorption energy of CO at the cluster hollow position, 1.77 eV (Table 1), is about 0.3 eV larger than the experimental value for the single-crystal Pd(111) surface at a low coverage, 1.47−1.54 eV.[50,51] The functional BP86 is known to overestimate binding energies whereas the energies calculated with the more recent functional PBEN are usually more accurate.[52,53] The present study also supports this finding: the PBEN//BP86 adsorption energy for CO on Pd_{146}, 1.49 eV (Table 1), reproduces the experimental value of 1.47−1.54 eV with "chemical" accuracy. Thus, by combining three-dimensional cluster models, proposed here, and accurate exchange-correlation potentials, e.g., PBEN, it should be possible to calculate adsorption energies in *quantitative agreement* with experiment.

The O_h symmetry constraints do not allow us to consider bridge positions of cluster (111) facets in the same way as for 3-fold and on-top positions. To compare these three adsorption positions we used an alternative scheme of the adsorbate location where three CO molecules are placed on the (111) facet of Pd_{146} cluster, Figure 2. Unlike the just discussed structures with CO molecules adsorbed above the center of the facet, here the adsorption positions are closer to the cluster edges and corners. This vicinity of the cluster borders should affect the calculated

TABLE 2: Calculated Properties[a] of CO Adsorbed on Cluster Edges, Kinks, and (001) Facet

	bridge	on-top			4-fold	
	$Pd_{146}(CO)_{12}$	$Pd_{146}(CO)_6$	$Pd_{148}(CO)_8$	$Pd_{116}(CO)_6$	$Pd_{140}(CO)_6$	$Pd_{147}(CO)_6$
r(C−O), Å	1.175	1.154	1.154	1.153	1.198	1.193
r(Pd−C), Å	1.982	1.885	1.883	1.875	2.229	2.248
D_e(BP86),[b] eV	1.95	1.43	1.46	1.23 (1.00)	1.54	1.50
ν_e(C−O), cm^{-1}	1859	1997	1988	2004	1656	1687
ν_e(C−O) × 1.04, cm^{-1}	1933	2076	2068	2084	1722	1754

[a] For the designation of the various properties, see Table 1. [b] Adsorption energy D_e(PBEN//BP86) calculated with PBEN exchange-correlation potential for the geometry optimized at the BP86 level given in parentheses.

adsorption parameters. The "through-space" CO−CO interaction of 24 (free) CO molecules kept in the positions calculated for $Pd_{146}(CO)_{24}$ is very weak, ∼0.01 eV. Probably more important is that as many as four CO molecules adsorbed near each vertex of Pd_{146} octahedron interact with a rather small part of Pd_{146} moiety. Thus, the adsorbate−substrate charge transfer in this arrangement may not be sufficiently compensated by the rest of the cluster as in the case with one CO molecule per facet. Actually, calculations of $Pd_{146}(CO)_{24}$ cluster (Table 1) yield a small decrease of adsorption energy for 3-fold and on-top positions, accompanied by an elongation of the Pd−CO distance; consistently, the C−O vibrational frequency shifts to higher values. However, the most important finding is that the relative strength of the adsorption positions for $Pd_{146}(CO)_{24}$ follows the same order as on the ideal Pd(111) surface: hollow > bridge > on-top. Almost quantitative agreement is found (Table 1): the BP86 (PBEN) adsorption energy for the hollow position is by 0.22 eV (0.20 eV) and 0.54 eV (0.46 eV) higher than for the bridge and on-top positions, respectively; the corresponding slab model PW91 values are 0.17 and 0.64 eV.[15] Hence, at least at low CO coverage, the adsorption positions at the regular (111) facets of Pd nanoparticles are calculated to be occupied in the same preference sequence as for ideal Pd(111) surface: 3-fold hollow sites are energetically favored over bridge sites and, even more so, over on-top sites. Note that the calculated reduction, at most 10%, of the CO adsorption energy on the 3-fold hollow sites of relaxed clusters up to Pd_{140} with shorter Pd−Pd distances[16] (see also Subsection 4.1.2) does not change the aforementioned preference sequence. The effect of the cluster morphology on the properties of adsorption sites of its (111) facets is thus insignificant.

4.1.2. CO Adsorption at Cluster Edges, Corners, and Defects. The adsorption positions different from those located at regular cluster facets are assumed to be responsible for the observed differences between Pd nanoparticles and a well-prepared ("ideal") Pd(111) surface.[10,11] Let us consider first the adsorption of CO at the edges of the cluster Pd_{146}. If a single CO molecule is adsorbed at the bridge position in the middle of each cluster edge, then O_h symmetry is preserved and the whole system is described by the formula $Pd_{146}(CO)_{12}$. Such a bridge site at the cluster edge exhibits a CO adsorption energy of 1.95 eV at the BP86 level (Table 2). This is the strongest binding of CO calculated in the present study. Compared to the bridge site at the (111) facet (Table 1), the notably stronger interaction with the cluster edge is also reflected in the geometry: for the bridge-on-edge complex, the Pd−C distance is shorter and the C−O bond is slightly longer. Such changes are in agreement with the general mechanism of CO bonding at metal surfaces described by electron donation from metal to the antibonding $2\pi^*$ orbital of CO and back-donation from the bonding 5σ orbital of CO to the metal.

In Section 4.1.1 we demonstrated that the adsorption properties of regular (111) facets of Pd nanoparticles are close to those of ideal Pd(111) surface, i.e., at low CO coverage only 3-fold hollow sites should preferentially be populated at cluster facets. The strong bond found here for the bridge-on-edge position might explain the signal corresponding to the vibration of a CO molecule adsorbed at a bridge site that appears under UHV conditions in IRAS[54,55] and SFG spectra of supported Pd nanoparticles (and/or a high-defect Pd(111) surface[10,11]), as shown below.

Adsorption at cluster corners (cluster $Pd_{146}(CO)_6$, Table 2) exhibits a binding energy that is by ∼0.3 eV higher than that for on-top positions at the (111) cluster facets (Table 1) although the geometries of the adsorption complexes are very similar. Obviously, a stronger bond is formed with the low-coordinated Pd center: the corner atoms are four-coordinated, while the Pd centers at regular (111) facets exhibit coordination number 9.

The corner position considered here is probably an oversimplified model, as the ideal octahedral shape of the supported Pd clusters is unlikely formed under experimental conditions. The surface of Pd nanoparticles exposes numerous defects such as steps and kinks.[4,10] Also, to some extent a corner position represents kinks at a (001) surface. As a model of a defect at the (111) facet, we investigated the Pd_{148} cluster (Figure 1) that is obtained from Pd_{140} by deposition of an additional Pd atom at the central hollow site of each (111) facet. CO is adsorbed on-top of these three-coordinated Pd centers (cluster $Pd_{148}(CO)_8$, Table 2). The calculated adsorption parameters are very close to those for adsorption at corner sites. The adsorption energy of 1.46 eV (BP86) is as large as for the bridge position at the regular (nondefect) (111) facet.

Next, we address an important aspect of metal clusters: the influence of structure relaxation of clusters on the properties of adsorption sites. The calculated average interatomic distance of three-dimensional metal clusters is known to increase with cluster size.[56−59] This trend is described by an approximately linear dependence of the average interatomic distance on the average coordination number. For clusters of about 150 atoms, the average interatomic distance $\bar{r}$(Pd−Pd) still differs notably from the value corresponding to the bulk crystal.[56−59] For instance, the cluster Pd_{140} optimized at the VWN level features $\bar{r}$(Pd−Pd) = 2.68 Å, whereas extrapolation to the bulk yields 2.73 Å. (The latter value is slightly smaller than the experimental value of 2.75 Å.[16])

It is an empirical finding that, for reasonably strong bonds, LDA (VWN) structural results often agree better with experiment than results obtained with GGA functionals; the latter, in turn, yield much more accurate thermochemistry results including adsorption energies.[60,61] Recently, we studied the effect of the cluster geometry on CO adsorption at the 3-fold hollow sites located at the center of (111) facets.[16] We considered two types of cluster geometries: a bulk terminated fixed geometry with r(Pd−Pd) = 2.75 Å, as used throughout the present work, and cluster geometries that were fully optimized for bare clusters at the VWN level. For the series of octahedral clusters, Pd_{79}, Pd_{85}, Pd_{116}, and Pd_{140}, only a small decrease of the adsorption energy D_e(BP86) by less than 0.2 eV (or ∼10%) was computed

when going from the fixed cluster geometry to the VWN optimized geometry.[16] Slab model calculation also indicate a weak dependence of Pd(111) surface adsorption properties on the Pd−Pd distance in the range 2.75−2.86 Å.[15] However, low-coordinated Pd centers may be more sensitive to the local structure of adsorption sites, thus making it more important to account for cluster relaxation.

To examine this hypothesis, the structure of the Pd_{148} cluster was optimized using the VWN approach in two steps (within the constraints of O_h symmetry). First, the positions of the defect Pd centers on the (111) facets were relaxed. As a result, the distances between the defect atom and the Pd centers forming a 3-fold hollow site beneath it decreased notably, from the previously fixed value of 2.75 to 2.63 Å. The energy of CO adsorption on-top of defect Pd atom was reduced to 1.38 eV, compared to the initial value of 1.46 eV (Table 2). In the next step, the cluster geometry was fully relaxed; this caused only minor changes in the local environment of the defect center. For instance, the CO binding decreased further, to 1.35 eV. Thus, the overall effect of cluster relaxation on the adsorption energy is ∼0.1 eV, even in the case of a low-coordinated Pd center.

4.1.3. CO Adsorption at (001) Facets. It is assumed that well-prepared Pd nanonparticles deposited on alumina films exhibit only a small fraction of (001) facets.[4,10,11] Nevertheless, we considered the adsorption of CO at these facets as well. On the Pd(001) surface, only bridge-adsorbed CO was detected experimentally for a broad range of coverages,[62,63] however, a partial occupation of the 4-fold hollow sites was predicted at low coverage.[64] At low coverage ($\theta = 0.006$), bridge-bonded CO is characterized by a C−O vibrational frequency of 1895 cm^{-1}.[63] The measured binding energy extrapolated to zero coverage is 1.55 eV; it decreases linearly with growing CO coverage to ∼1.3 eV at $\theta = 0.45$.[65] According to another measurement, the heat of CO adsorption on Pd(001), 1.67 eV, is constant up to the coverage of $\theta = 0.45$.[64] However, slab model calculations of the ordered structure c(2 × 2) corresponding to $\theta = 0.5$ show that the 4-fold hollow adsorption site is by 0.10 (BP86) or 0.13 eV (PW91) more stable than the bridge position.[66] Similar to the Pd(111) surface, on-top adsorbed CO shows the weakest binding on Pd(001).[66]

For (001) facets, we investigated two types of 4-fold hollow sites: the site of the cluster Pd_{140} which is obtained by removing six corner atoms from the cluster Pd_{146} and the position at the center of (001) facets of the cluster Pd_{147} (Figure 1). At Pd_{140}, (001) facet are formed by only four Pd centers with coordination number 6. The cluster Pd_{147} exhibits a more extended fragment of the (001) surface and the central hollow site is formed by eight-coordinated Pd atoms. Nevertheless, very similar results were obtained for the 4-fold positions of both clusters, $Pd_{146}(CO)_6$ and $Pd_{147}(CO)_6$ (Table 2). The BP86 adsorption energy at the hollow site of ∼1.5 eV is slightly higher than the value of 1.4 eV calculated with the same functional for a two-layer Pd(001) slab model.[66] The calculated energies fall into the range of experimental estimates.[65] The geometry characteristics, for instance of the $Pd_{147}(CO)_6$ system, namely the C−O bond length of 1.19 Å and the Pd−C distance of 2.25 Å, are also very similar to the corresponding values calculated for the slab model, 1.18 and 2.28 Å.[66]

We also considered on-top adsorption the (001) facet of the cluster Pd_{116} (Figure 1). The calculated adsorption energy is by ∼0.3 eV smaller than for the hollow site; the same result was reported for slab model calculations.[66] The geometry characteristics are again very similar: the C−O bond length of 1.15 Å coincides for cluster and slab models; the Pd−C distance of 1.88 Å for the cluster is only slightly shorter than for the slab model, 1.91 Å.

Summarizing our results for various on-top adsorption sites studied, one can distinguish two types of such sites: (i) on-top positions on the regular (111) and (001) facets with weak binding, and (ii) defect low-coordinated Pd centers exhibiting a relatively strong adsorption bond with CO (due to steric as well as chemical effects). The latter sites are available for adsorption already at low coverage, while the former should be populated only at high pressure due to competition with stronger attractive hollow and bridge sites.

Unfortunately, adsorption of CO at a bridge site of (001) cluster facets can be considered only when the octahedral symmetry of present cluster models is broken. Alternatively, much large cluster models should be used with (001) facets large enough for depositing several (at least four) CO molecules. Both, lower symmetry or larger cluster size, will lead to a significantly larger computational effort. However, on the basis of the very good agreement for hollow and on-top sites between calculations of cluster models on one hand and slab models on the another, one should expect rather similar results also for bridge positions that, according to slab model calculations, exhibit slightly weaker, by 0.1 eV, binding with CO than 4-fold hollow sites.[66] Such a small difference between hollow and bridge sites of the (001) surface lies at the accuracy limit of the computational method. Also, only the C−O vibration corresponding to bridge positions is experimentally observed, even at very low coverage;[63] this indicates that bridge positions are more stable on this surface. In summary, as in the case of (111) cluster facets, the properties of adsorption sites on (001) nanocluster facets are very similar to the characteristics of the ideal Pd(001) surface—despite the relatively small facet size of the cluster models used. In general, CO binding on (001) facets is slightly weaker than on (111) facets.

4.2. Calculated Vibrational Frequencies of CO Adsorbed on Pd Nanoparticles. The harmonic vibrational frequencies calculated at the GGA-BP86 level are by 3−4% smaller than the experimental (anharmonic) values. For instance, $\nu_e(C-O) = 1755\ cm^{-1}$ is calculated for the 3-fold hollow position located at the center of (111) facets of the cluster Pd_{146} (Table 1); this is to be compared to 1808−1825 cm^{-1} measured at very low CO coverage on Pd(111).[67,68] Such a notable frequency underestimation in gradient-corrected DF calculations is consistent with the overestimation of interatomic distances mentioned above; this is a general feature of common GGA exchange-correlation potentials, in particular when dealing with bonds involving transition metal and other heavy atoms.[60,61] To facilitate comparison with experimental vibrational spectra, we introduce a scaling factor of 1.04 chosen so that it adjusts the calculated frequency of CO on 3-fold hollow site to the value of 1825 cm^{-1}, measured for CO adsorbed at Pd(111).[69] The scaled frequencies (Tables 1 and 2) fall into four groups, depending on the type of the adsorption position. The lowest C−O frequency around 1720 cm^{-1} (the highest red shift compared to gas-phase CO, 2143 cm^{-1}) corresponds to 4-fold sites on (001) facets. Next are 3-fold hollow sites with frequencies in the interval 1825−1875 cm^{-1} and bridge sites, 1933−1951 cm^{-1}. On-top sites with vibrational frequencies in the range 2066−2092 cm^{-1} exhibit the smallest shift.

Little is known about the occupation of 3- and 4-fold sites at (111) and (001) facets, respectively, of alumina-supported Pd nanoparticles.[10,11] Comparison of the systems $Pd_{146}(CO)_8$ and $Pd_{146}(CO)_{24}$ (Table 1) shows that the frequency of CO molecules

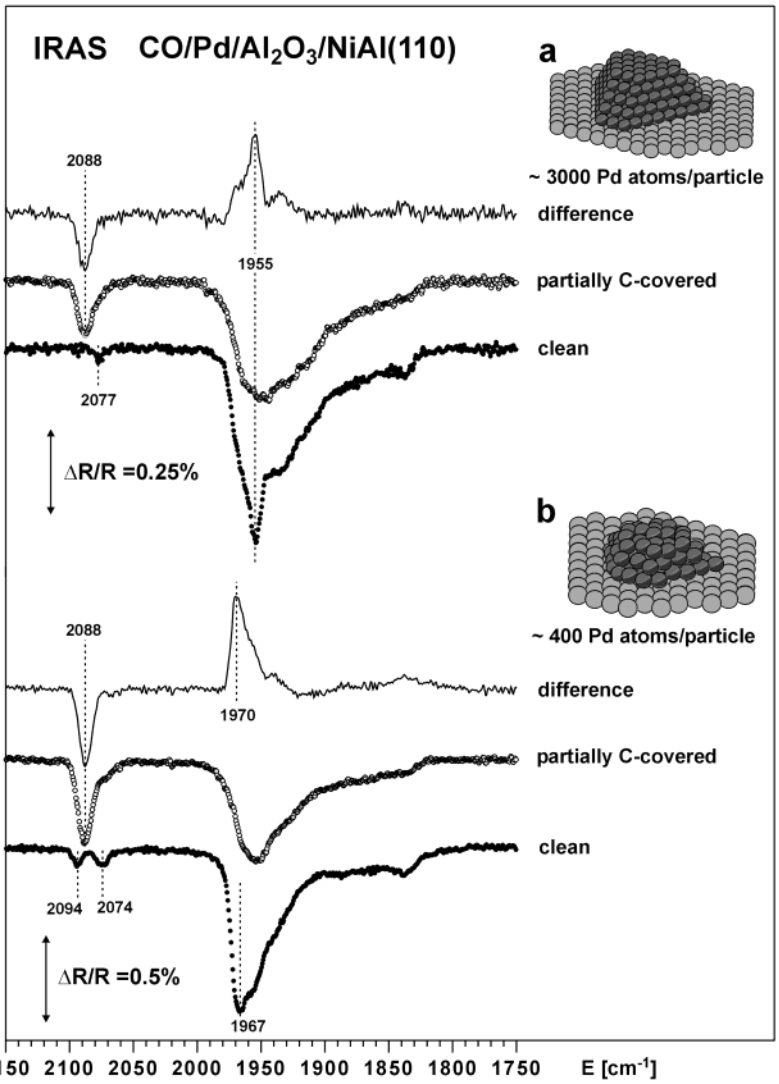

Figure 3. IR reflection absorption spectra of the CO stretching frequency region for Pd particles of different size and structure supported on Al_2O_3/NiAl(110). The spectra were taken at a sample temperature of 100 K after CO exposure at 300 K (about 20 L). Solid symbols: clean particles immediately after preparation; open symbols: partially carbon-covered particles after extended exposure to methanol at 440 K; solid line: difference spectrum for the two situations.

occupying 3-fold hollow sites can vary significantly, depending on the environment of this site at the (111) facet: from 1825 cm^{-1} for CO in the center of the facet to 1875 cm^{-1} in the hollow close to cluster edges. The higher frequency for the latter site is consistent with the weaker binding energy (by 0.1 eV) at this site. On-top sites of the (111) facet also follow this trend: the CO frequency of on-top sites near a cluster edge, 2092 cm^{-1}, is by 26 cm^{-1} higher than that of the on-top site in the center of (111) facets; see the values for the cluster $Pd_{147}(CO)_8$ (Table 1).

O_h symmetry constraints did not allow us to consider bridge adsorption sites remote from cluster edges. Yet, based on the results for 3-fold and on-top sites, a frequency shift of about 40 cm^{-1} can be assumed for bridge sites when moving from the center of (111) facets to cluster borders. Thus, at the same theoretical level, based on the calculated result for the bridge positions at $Pd_{146}(CO)_{24}$ (Table 1), the vibrational frequency for bridge-bonded CO on perfect Pd(111) should be close to 1910 cm^{-1}. This value is red-shifted with respect to 1933 cm^{-1}, calculated for bridge sites at cluster edges (Table 2). This is in qualitative agreement with the experimental findings: the frequency measured for the bridge site of the ideal Pd(111) surface, 1955 cm^{-1},[10] is lower than for bridge sites on supported clusters, 1977 cm^{-1}.[6,10,11] From this argument, it follows that the cluster $Pd_{146}(CO)_{24}$, with a calculated frequency of 1951 cm^{-1} for bridge-adsorbed CO apparently is not a very good model for Pd(111).

On the basis of the results of adsorption energy calculations (Section 4.1) we assign the experimentally observed vibration of CO adsorbed at bridge and on-top positions of supported Pd nanoparticles to bridge sites at cluster edges and low-coordinated on-top positions, respectively. Despite the scaling correction, the calculated frequencies for bridge-on-edge, 1933 cm^{-1}, and low-coordinated on-top sites, 2068−2076 cm^{-1}, still seem to be somewhat underestimated when compared to the experimental values of 1950−1975 cm^{-1} and 2077−2090 cm^{-1} for supported Pd nanoparticles at low CO pressure. The experimental observations will be described in the next section.

4.3. IRAS and SFG Studies of CO Adsorption on Pd Nanoclusters. To correlate theoretical findings with experimental results, we investigated the adsorption of CO employing vibrational spectroscopies over a broad range of partial pressures.

We start by considering the vibrational properties of adsorbed CO in the UHV region. Here, two types of Pd nanoparticles were chosen (Figure 3). The first type (Figure 3a) were large

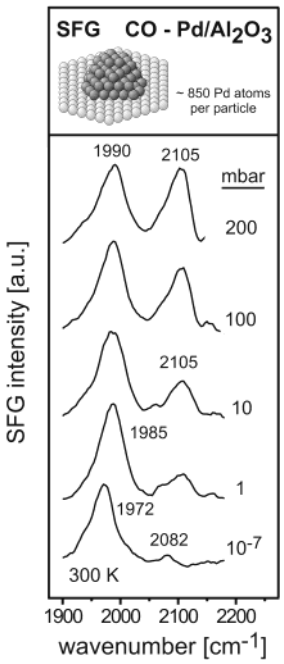

Figure 4. SFG spectra of CO adsorption on Al_2O_3-supported Pd nanoparticles (mean size 3.5 nm) at 300 K and between 10^{-7} and 200 mbar.

and ordered Pd crystallites with an average diameter of ~6 nm (containing approximately 3000 Pd atoms per particle). These nanocrystallites grow in (111)-orientation, preferentially exposing (111) facets as well as a small fraction of (100) facets. As a second type (Figure 3b), we investigated Pd aggregates with an average size of ~3 nm (containing about 400 atoms per particle). On these smaller aggregates no indications for the formation of ordered crystal facets could be found and it is assumed that their surface structure is characterized by a high density of defect sites. More details concerning the preparation and structure of the two model systems can be found in the literature.[4,10,47,48]

IRAS spectra were acquired for both types of model systems after CO saturation at 300 K. These spectra are displayed in Figure 3 (solid symbols). For the large, well-ordered particles (Figure 3a) a sharp and dominating absorption feature was observed in the CO stretching frequency region at approximately 1955 cm^{-1}. It has a broad low-frequency shoulder extending to approximately 1830 cm^{-1}. Additionally, a weak feature at 2077 cm^{-1} was observed. For the smaller and defect rich particles (Figure 3b) a similar spectrum is detected. A band at 1967 cm^{-1} dominates the absorption. On the low-frequency side down to approximately 1830 cm^{-1}, it extends into a shoulder containing several broad features. Furthermore, two weak bands in the high-frequency region were observed at 2074 cm^{-1} and at 2094 cm^{-1}.

Figure 4 shows corresponding SFG spectra of CO on Pd particles with a mean size of 3.5 nm (approximately 850 Pd atoms per particle) taken at 300 K. These particles were expected to have a defective structure similar to the particles shown in Figure 3b. In fact, the observed SFG resonances at 10^{-7} mbar at 1972 cm^{-1} and 2082 cm^{-1} were close to those in Figure 3b, and the small frequency shift may be rationalized by a slightly higher coverage due to the background pressure of 10^{-7} mbar CO.

To some extent, these spectra can be interpreted on the basis of single-crystal data[10] (and references therein). As already mentioned, on Pd(111), a large number of adsorbate structures are formed as a function of coverage. At low coverage, CO adsorbs in fcc hollow sites, changing to a mixture of fcc and hcp hollow sites at coverages up to 0.5.[70] Various ordered structures were observed in this region related to absorption features in the range between 1800 and 1920 cm^{-1}.[14,15,67,71] At coverage >0.5 ML, bridge-bonded species give rise to absorption in the range between 1960 and 1970 cm^{-1}.[14] However, under UHV conditions, this high-coverage regime is only accessible at low surface temperature. On Pd(100), CO absorption features in the region from 1895 cm^{-1} to 1997 cm^{-1} were observed.[63]

Based on these data, the series of broad features in the range between 1830 cm^{-1} and 1930 cm^{-1} can be assigned to CO mainly adsorbed at hollow sites on Pd(111) facets. The absorption peaks at 2077 cm^{-1} (6 nm particles), 2082 cm^{-1} (3.5 nm particles), 2074 cm^{-1} (3 nm particles), and 2094 cm^{-1} (3 nm particles) are related to CO adsorbed in on-top geometry. It is likely that the feature is at least partially related to defect sites. Of specific interest with respect to the present study are the dominating features at 1955 cm^{-1} (6 nm particles) and ~1970 cm^{-1} (smaller particles). As discussed previously, the band may be assigned to bridge-bonded CO either on (100) facets or at defect sites such as particle edges or steps.[7,10,11] Taking into account the specific morphology of the large ordered particles, the contribution of (100) facets is expected to be minor, however. For, the fraction of these facets is small and their orientation with respect to the surface normal is tilted, reducing the parallel component of the dynamic dipole moment (note that the metal surface selection rule is valid on metal particles supported on thin oxide films[67]).

On the basis of these considerations and the results of the present DF calculations indicating strong bonding of CO to bridge sites at particles edges, the features at 1955 cm^{-1} and ~1970 cm^{-1} are assigned to bridge-bonded CO adsorbed at particle-defect and edge sites. One expects that on the large and ordered particles regular edges are the dominating type of defect sites, whereas on smaller particles a broader spectrum of edge-like positions with different local structure exists. Finally, all the spectral features observed are expected to be strongly modified by dipole coupling effects. As a consequence, the relative intensities do not directly reflect the relative fraction of CO adsorbed at the corresponding sites, but the defect band at high frequency is expected to gain intensity on the expense of the lower frequency features.[7,54]

The assignment of the absorption bands at 1955 cm^{-1} and 1967 cm^{-1} is corroborated by IR spectra acquired from partially carbon-covered surfaces. This surface carbon is produced by extended exposure to methanol at a sample temperature of 440 K (see refs 23 and 24 for details). Under these conditions, slow C−O bond scission leads to the buildup of adsorbed carbon. The corresponding IR spectra after subsequent CO saturation at 300 K for the two types of Pd particles are displayed in Figure 3 (open symbols). In addition, the difference spectra for CO on the clean and on the partially carbon-covered samples are shown. It is found that specifically the defect features are affected by adsorbed carbon. In contrast to this, the spectral region assigned to regular Pd(111) facets (1930 cm^{-1} and 1830 cm^{-1}) is hardly modified. This interpretation is consistent with the assumption that the edge and defect sites on the Pd particles are characterized by adsorption and reaction properties which differ from the regular facets. As soon as the preferred adsorption sites at the particle defects are blocked, CO is forced to adsorb in an on-top geometry, giving rise to the new absorption feature at 2088 cm^{-1}.

The high-pressure behavior of the model catalyst was examined using SFG (for details see refs 6 and 10). With increasing pressure the defect-related features shifted to higher wavenumber and the on-top peak increased in intensity (Figure 4). This can be understood by considering that more on-top sites were populated with increasing coverage together with the effect of dipole coupling (in agreement with single-crystal SFG data[10]). Apparently, at 200 mbar CO the defect-related species was still present, together with a considerable fraction of on-top CO.

5. Conclusions

Adsorption of CO molecules on nanosize three-dimensional Pd particles of about 150 atoms, exhibiting (111) and (001) facets, was studied computationally by means of an all-electron scalar relativistic density functional method. The calculated results show that adsorption properties of rather small (111) and (001) cluster facets are similar to the properties of the corresponding ideal (infinite) Pd surfaces. In particular, on regular (111) facets of Pd clusters, CO adsorption at 3-fold hollow positions is energetically preferred compared to bridge and on-top sites, just as at the ideal Pd(111) surface. This conclusion is also valid for adsorption sites in the vicinity of cluster edges and corners.

However, the strongest CO bonding is calculated at bridge positions of cluster edges where the adsorbate binds to low-coordinated Pd centers. Consequently, at low CO pressures, the irregular adsorption sites at cluster edges are expected to be occupied first. Therefore, the signal from bridge-bonded CO ($\sim$1975 cm^{-1}) is observed for supported Pd clusters already at 10^{-7} mbar.[6,10,11]

On-top adsorption on low-coordinated Pd centers (cluster corners and surface kinks) is calculated stronger than at on-top positions of regular (111) and (100) facets. This rationalizes the experimental observation that occupation of on-top positions on smaller and defect-rich supported Pd nanoparticles starts at much lower CO pressures than on the larger well-faceted particles.[10,11]

The theoretical results were compared to vibrational spectra of CO on different types of Pd nanoparticles, supported on a well-ordered Al_2O_3 film on NiAl(110), obtained by IR reflection absorption spectroscopy (IRAS) under UHV conditions and sum frequency generation (SFG) spectroscopy in the mbar pressure range. A dominating absorption band in the frequency region between 1955 cm^{-1} and 1970 cm^{-1} was observed, which on the basis of the theoretical results was assigned to CO adsorbed in a bridge-bonded geometry at particle edges and at edge-like defect sites. SFG was able to demonstrate that the defect-related bridge species also occurred in a high-pressure gas environment, typical of catalytic reactions. On partially carbon-covered Pd particles prepared by methanol decomposition, IRAS indicated that the adsorption at edge sites is strongly modified and CO adsorbed in an on-top geometry instead.

Acknowledgment. This work was supported by the Deutsche Forschungsgemeinschaft, and the Fonds der Chemischen Industrie.

References and Notes

(1) Haberland, H., Ed. *Clusters of Atoms and Molecules*; Vol. 1, Springer Series in Chemical Physics, Vol. 52, Springer: Berlin, 1994.
(2) Braunstein, P., Oro, L. A., Raithby, P. R., Eds. *Metal Clusters in Chemistry*; Wiley-VCH: Weinheim, 1999; Vols. 2 and 3.
(3) Rösch, N.; Pacchioni, G. In *Clusters and Colloids—From Theory to Applications*; Schmid, G., Ed.; Verlag Chemie: Weinheim, 1994; p 5.
(4) Bäumer, M.; Freund, H.-J. *Prog. Surf. Sci.* **1999**, *61*, 127.
(5) Henry, C. R. *Surf. Sci. Rep*. **1998**, *31*, 231.
(6) Dellwig, T.; Rupprechter, G.; Unterhalt, H.; Freund, H.-J. *Phys. Rev. Lett.* **2000**, *85*, 776.
(7) Frank, M.; Bäumer, M. *Phys. Chem. Chem. Phys.* **2000**, *2*, 3723.
(8) Libuda, J.; Meusel, I.; Hoffmann, J.; Hartmann, J.; Piccolo, L.; Henry, C. R.; Freund, H.-J. *J. Chem. Phys.* **2001**, *114*, 4669.
(9) Rupprechter, G. *Phys. Chem. Chem. Phys.* **2001**, *3*, 4621.
(10) Unterhalt, H.; Rupprechter, G.; Freund, H.-J. *J. Phys. Chem. B* **2002**, *106*, 356.
(11) Rupprechter, G.; Unterhalt, H.; Morkel, M.; Galletto, P.; Hu, L.; Freund, H.-J. *Surf. Sci.* **2002**, *502*−*503*, 109.
(12) Giorgi, J. B.; Schroeder, T.; Bäumer, M.; Freund, H.-J. *Surf. Sci.* **2002**, *498*, L71.
(13) Gotti, A.; Prins, R. *J. Catal*. **1998**, *175*, 302.
(14) Tüshaus, M.; Berndt, W.; Conrad, H.; Bradshaw, A. M.; Persson, B. *Appl. Phys. A* **1990**, *51*, 91.
(15) Loffreda, D.; Simon, D.; Sautet, P. *Surf. Sci.* **1999**, *425*, 68.
(16) Yudanov, I. V.; Sahnoun, R.; Neyman, K. M.; Rösch, N. *J. Chem. Phys*. **2002**, *117*, 9887.
(17) Freund, H.-J. *Surf. Sci.* **2002**, *500*, 271.
(18) Freund, H.-J.; Bäumer, M.; Kuhlenbeck, H. *Adv. Catal*. **2000**, *45*, 333.
(19) Freund, H.-J. *Angew. Chem., Int. Ed. Engl.* **1997**, *36*, 452.
(20) Jaeger, R. M.; Kuhlenbeck, H.; Freund, H.-J.; Wuttig, M.; Hoffmann, W.; Franchy, R.; Ibach, H. *Surf. Sci.* **1991**, *259*, 235.
(21) Libuda, J.; Winkelmann, F.; Bäumer, M.; Freund, H.-J.; Bertrams, T.; Neddermeyer, H.; Müller, K. *Surf. Sci*. **1994**, *318*, 61.
(22) Libuda, J.; Freund, H.-J. *J. Phys. Chem. B* **2002**, *106*, 4901.
(23) Schauermann, S.; Hoffmann, J.; Johánek, V.; Hartmann, J.; Libuda, J. *Phys. Chem. Chem. Phys.* **2002**, *4*, 3909.
(24) Schauermann, S.; Hoffmann, J.; Johánek, V.; Hartmann, J.; Libuda, J.; Freund, H.-J. *Angew. Chem., Int. Ed.* **2002**, *41*, 2513.
(25) Dunlap, B. I.; Rösch, N. *Adv. Quantum Chem*. **1990**, *21*, 317.
(26) Belling, T.; Grauschopf, T.; Krüger, S.; Mayer, M.; Nörtemann, F.; Staufer, M.; Zenger, C.; Rösch, N. In *High-Performance Scientific and Engineering Computing*; Bungartz, H.-J., Durst, F., Zenger, C., Eds.; Lecture Notes in Computational Science and Engineering, Vol. 8; Springer: Heidelberg, 1999; p 439.
(27) Belling, T.; Grauschopf, T.; Krüger, S.; Nörtemann, F.; Staufer, M.; Mayer, M.; Nasluzov, V. A.; Birkenheuer, U.; Hu, A.; Matveev, A. V.; Shor, A. M.; Fuchs-Rohr, M. S. K.; Neyman, K. M.; Ganyushin, D. I.; Kerdcharoen, T.; Woiterski, A.; Rösch, N. *ParaGauss*, Version 2.2; Technische Universität München, 2001.
(28) Häberlen, O. D.; Rösch, N. *Chem. Phys. Lett.* **1992,** *199*, 491.
(29) Rösch, N.; Krüger, S.; Mayer, M.; Nasluzov, V. A. In *Recent Developments and Applications of Modern Density Functional Theory*; Seminario, J. M., Ed.; Elsevier: Amsterdam, 1996; p 497.
(30) Vosko, S. H.; Wilk, L.; Nusair, M. *Can. J. Phys*. **1980**, *58*, 1200.
(31) Becke, A. D. *Phys. Rev. A* **1988**, *38*, 3098.
(32) Perdew, J. P. *Phys. Rev. B* **1986**, *33*, 8622; **1986**, *34*, 7406.
(33) Fan, L.; Ziegler, T. *J. Chem. Phys*. **1991**, *94*, 6057.
(34) Hammer, B.; Hansen, L. B.; Nørskov, J. K. *Phys. Rev. B* **1999**, *59*, 7413.
(35) Huzinaga, S. *J. Chem. Phys*. **1977**, *66*, 4245.
(36) Widmark, P.-O.; Malmqvist, P.-A.; Roos, B. O. *Theor. Chim. Acta* **1990**, *77*, 291.
(37) *CRC Handbook of Chemistry and Physics*, 77th ed.; Lide, D. R., Ed.; CRC Press: Boca Raton, 1996.
(38) Nasluzov, V. A.; Rösch, N. *Chem. Phys*. **1996**, *210*, 413.
(39) Nörtemann, F. Dissertation, Technische Universität München, 1998.
(40) Boys, S. F.; Bernardi, F. *Mol. Phys*. **1970**, *19*, 553.
(41) *Cluster Models for Surface and Bulk Phenomena;* Pacchioni, G., Bagus, P. S., Parmigiani, F., Eds.; NATO ASI Series B, Vol. 283, Plenum: New York, 1992.
(42) Whitten, J. L.; Yang, H. *Surf. Sci. Rep.* **1996**, *24*, 59.
(43) Libuda, J.; Meusel, I.; Hartmann, J.; Freund, H.-J. *Rev. Sci. Instrum*. **2000**, *71*, 4395.
(44) Rupprechter, G.; Dellwig, T.; Unterhalt, H.; Freund, H.-J. *Top. Catal.* **2001**, *15*, 19.
(45) Somorjai, G. A.; Rupprechter, G. *J. Phys. Chem. B* **1999**, *103*, 1623.
(46) Jaeger, R. M.; Libuda, J.; Bäumer, M.; Homann, K.; Kuhlenbeck, H.; Freund, H.-J. *J. Electron Spectrosc. Relat. Phenom*. **1993**, *64/65*, 217.
(47) Meusel, I.; Hoffmann, J.; Hartmann, J.; Libuda, J.; Freund, H.-J. *J. Phys. Chem. B* **2001**, *105*, 3567.
(48) Meusel, I.; Hoffmann, J.; Hartmann, J.; Heemeier, M.; Bäumer, M.; Libuda, J.; Freund, H.-J. *Catal. Lett*. **2001**, *71*, 5.
(49) Shaikhutdinov, S.; Heemeier, M.; Hoffmann, J.; Meusel, I.; Richter, B.; Bäumer, M.; Kuhlenbeck, H.; Libuda, J.; Freund, H.-J.; Oldman, R.; Jackson, S. D.; Konvicka, C.; Schmid, M.; Varga, P. *Surf. Sci*. **2002**, *501*, 270.
(50) Bradshaw, A. M.; Hoffmann, F. M. *Surf. Sci.* **1978**, *72*, 513.
(51) Guo, X.; Yates, J. T., Jr. *J. Chem. Phys.* **1989**, *90*, 6761.
(52) Lopez, N.; Nørskov, J. K. *Surf. Sci.* **2001**, *477*, 59.

(53) Matveev, A.; Staufer, M.; Mayer, M.; Rösch, N. *Int. J. Quantum Chem*. **1999**, *75*, 863.
(54) Wolter, K.; Seiferth, O.; Kuhlenbeck, H.; Bäumer, M.; Freund, H.-J. *Surf. Sci*. **1998**, *399*, 190.
(55) Frank, M.; Bäumer, M. *Phys. Chem. Chem. Phys*. **2000**, *2*, 3723.
(56) Pacchioni, G.; Chung, S.-C.; Krüger, S.; Rösch, N. *Chem. Phys*. **1994**, *184*, 125.
(57) Häberlen, O.; Chung, S.-C.; Stener, M.; Rösch, N. *J. Chem. Phys*. **1997**, *106*, 5189.
(58) Krüger, S.; Vent, S.; Rösch, N. *Ber. Bunsen-Ges. Phys. Chem*. **1997**, *101*, 1640.
(59) Krüger, S.; Vent, S.; Nörtemann, F.; Staufer, M.; Rösch, N. *J. Chem. Phys*. **2001**, *115*, 2082.
(60) Ziegler, T. *Chem. Rev.* **1991**, *91*, 651.
(61) Görling, A.; Trickey, S. B.; Gisdakis, P.; Rösch, N. In *Topics in Organometallic Chemistry*, Vol. 4; Brown, J., Hofmann P., Eds.; Springer: Heidelberg, 1999; p 109.
(62) Hoffmann, F. M. *Surf. Sci. Rep*. **1983**, *3*, 107.
(63) Ortega, A.; Hoffmann, F. M.; Bradshaw, A. M. *Surf. Sci*. **1982**, *119*, 79.
(64) Behm, R. J.; Christmann, K.; Ertl, G.; van Hove, M. A. *J. Chem. Phys*. **1980**, *73*, 2984.
(65) Tracy, J. C.; Palmberg, P. W. *J. Chem. Phys*. **1969**, *51*, 4852.
(66) Delbecq, F.; Sautet, P. *Phys. Rev. B* **1999**, *59*, 5142.
(67) Hoffmann, F. M. *Surf. Sci. Rep*. **1983**, *3*, 107.
(68) Kuhn, W. K.; Szanyi, J.; Goodman, D. W. *Surf. Sci. Lett*. **1992**, *274*, L611.
(69) Scaling of vibrational frequencies is not a universal measure; rather, it seems to be applicable only to a narrow range of similar systems. For instance, the calculated (harmonic) vibrational frequency of a free CO molecule results in a value of 2198 cm^{-1} when scaled by 1.04, an overestimation of the experimental anharmonic value by as much as 55 cm^{-1}. Alternatively, comparison with experiment could be facilitated by invoking a constant positive frequency shift by 70 cm^{-1}.
(70) Giessel, T.; Schaff, O.; Hirschmugl, C. J.; Fernandez, V.; Schindler, K.-M.; Theobald, A.; Bao, S.; Lindsay, R.; Berndt, W.; Bradshaw, A. M.; Baddeley, C.; Lee, A. F.; Lambert, R. M.; Woodruff, D. P. *Surf. Sci*. **1998**, *406*, 90.
(71) Ortega, A. Dissertation, Technische Universität Berlin, 1980.